Solid State Communications 152 (2012) 1829–1833

Contents lists available at SciVerse ScienceDirect

Solid State Communications

journal homepage: www.elsevier.com/locate/ssc

In-situ mechanical characterization of wurtzite InAs nanowires

Róbert Erdélyi [a,b,*], Morten Hannibal Madsen [c], György Sáfrán [a], Zoltán Hajnal [a], István Endre Lukács [a], Gergő Fülöp [d], Szabolcs Csonka [d], Jesper Nygård [c], János Volk [a]

[a] Research Centre for Natural Sciences, Institute of Technical Physics and Materials Science, 1025 Budapest, Pusztaszeri út 59-67, Hungary
[b] University of Pannonia, Faculty of Information Technology, Doctoral School of Molecular- and Nanotechnologies, 8200 Veszprém, Egyetem út 10, Hungary
[c] University of Copenhagen, Niels Bohr Institute, Nano-Science Center, 2100 Copenhagen, Denmark
[d] Budapest University of Technology and Economics, Department of Physics, 1111 Budapest, Budafoki út 6, Hungary

ARTICLE INFO

Article history:
Received 13 May 2012
Received in revised form
22 June 2012
Accepted 1 July 2012
by M.S. Skolnick
Available online 14 July 2012

Keywords:
D. Young's modulus
E. Resonance excitation method
E. Finite element method
E. Sem micromanipulator

ABSTRACT

High aspect ratio vertical InAs nanowires were mechanically characterized in a scanning electron microscope equipped with two micromanipulators. One, equipped with a calibrated atomic force microscope probe, was used for in-situ static bending of single nanowires along the ⟨11–20⟩ crystallographic direction. The other one was equipped with a tungsten tip for dynamic resonance excitation of the same nanowires. This setup enabled a direct comparison between the two techniques. The crystal structure was analyzed using transmission electron microscopy, and for InAs nanowires with a hexagonal wutzite crystal structure, the bending modulus value was found to BM=43.5 GPa. This value is significantly lower than previously reported for both cubic zinc blende InAs bulk crystals and InAs nanowires. Besides, due to their high resonance quality factor ($Q > 1200$), the wurtzite InAs nanowires are shown to be a promising candidate for sub-femtogram mass detectors.

1. Introduction

There is a long-standing experimental interest in the mechanical properties of one dimensional nanostructures, e.g. nanowires (NWs), nanotubes, and nanorods (NRs), because of their potential applications in sensors, actuators, and energy harvesting devices. However, the experimental results on the basic mechanical parameters are spreading in a surprisingly broad range. For instance the Young's modulus of II–VI semiconductor ZnO NWs or NRs with wurtzite structure was measured several times by a number of groups, but a conclusive value is still missing [1–8]. Especially important is the bending modulus (BM; i.e. the Young's modulus measured by bending) of cantilever beams in nanoelectromechanical systems. The most common method to determine the BM is the so called resonance excitation technique which was firstly demonstrated by Poncharal et al. They electrically induced oscillations in cantilevered, multiwalled carbon NTs in a transmission electron microscope (TEM) [9]. Manoharan et al. performed static bending experiments inside a scanning electron microscope (SEM) on individual ZnO NWs which were glued onto the specimen holder [7]. In this paper we present a combined in situ method to determine the BM of one dimensional cantilevered nanostructures. Although the resonance technique alone is suitable for BM measurement, we here apply this technique to validate the results of the static bending test. As an example we present the examination of high aspect ratio InAs NWs, however this method is not restricted to special materials. To our knowledge this is the first report of applying a static bending test and the resonance technique on the same individual, cantilevered nanostructures.

InAs is a III–V semiconductor, which has a number of parameters, such as direct band gap of 0.36 eV, electron mobility greater than $20.000\ cm^2\ V^{-1}\ s^{-1}$ at 300 K, strong spin-orbit interaction, Schottky-barrier free contacts, and gate tunable electron density, which makes it a good candidate for future nanoelectronics [10]. However, the number of reports about the mechanical observation of InAs cantilevered nanostructures is very limited. Mariager et al. excited three different acoustic oscillations of vertical InAs NWs by a femtosecond laser pulse [11]. Lexholm et al. studied the dynamic behavior of epitaxially grown InAs NWs with diameters ranging from 40 to 90 nm using optical stroboscopic imaging. They observed a decrease in Young's modulus with smaller diameters [12]. However, the crystal structure of their NWs was not examined in details, but claimed to go towards wurtzite for smaller diameters. InAs in bulk form always shows pure zinc-blende structure, nevertheless wurtzite InAs was observed for the first time by Koguchi et al. in nanowhiskers [13]. Caroff et al. showed that the crystal structure of InAs NWs can be controlled with NW diameter and the growth

* Corresponding author at: Research Centre for Natural Sciences, Institute of Technical Physics and Materials Science, 1025 Budapest, Pusztaszeri út 59-67, Hungary. Tel.: +36 1 392 2593; fax: +36 1 392 2226.
E-mail address: erdelyi.robert@ttk.mta.hu (R. Erdélyi).

0038-1098/$ - see front matter © 2012 Elsevier Ltd. All rights reserved.
http://dx.doi.org/10.1016/j.ssc.2012.07.005

temperature [14]. At small diameters the wurtzite structure is typical, and as the diameter is increased, mixed phases with different zinc-blende content or pure cubic structure can be achieved. By sidewall deposition during growth, Shtrikman et al. demonstrated a method to obtain thicker NWs with pure wurtzite crystal structure [15].

2. Experimental

The examined NWs were synthesized by solid source molecular beam epitaxy (MBE) on InAs(111)B substrates in a Varian GEN II MBE machine. The substrates were degassed at 250 °C for 1 h in a buffer chamber, and at 550 °C for 8 min, with an As backing pressure, immediately before applying gold. A thin layer of gold was evaporated at this elevated temperature and then annealed for 4 min. Hereafter the temperature was lowered to 445 °C, and the growth initialized by opening the In shutter. The wires were grown for 30 min at this temperature and for another 30 min with a temperature ramp to 455 °C. High flux rates of both In and As_2 was used, with beam equivalent pressures (BEP) of 7.0×10^{-7} Torr and 1.3×10^{-5} Torr, respectively, giving a V/III ratio of 19.

The crystal structure of the obtained nanostructures was examined by a JEOL JEM-3010 and a Phillips CM20 TEM. The morphology of the NWs was examined by a Zeiss 1540XB field emission SEM and the mechanical characterization was composed of two in situ successive measurements on the individual NWs in the SEM chamber. At first we carried out a static bending test on a randomly selected NW by an AFM cantilever mounted on a nanomanipulator arm (Kleindiek MM3A-EM). A soft silicon nitride cantilever (Veeco DNP-S20) was chosen to maximize the sensitivity of the method. Before mounting the nitride chip on the nanomanipulator arm, the spring constant was calibrated in an AFM (AIST-NT, SmartSPM 1010) using a reference Si cantilever. The NW was bent at its free end along the $\langle 11-20\rangle$ crystallographic direction by a lateral load perpendicular to the vertical axis by moving the sample with the stage towards the AFM tip. In order to maintain a permanent contact between the tip of the probe and the sidewall of the NW during manipulation, we etched an incision by focused ion beam (FIB) at the end of the tip with a radius of curvature comparable to the cross sectional radius of the NW. The schematic of the measurement and a typical SEM image recorded during the manipulation are shown in Fig. 1a and b, respectively. The inset of Fig. 1b shows the relative orientation of the applied bending load and the hexagonal cross section of the NW. For data acquisition, two snapshots were recorded during the bending: one in stressed and the other one in relaxed state. By overlapping the two snapshots, both NW and tip deflections could be determined (y and Y; Fig. 1a). No plastic deformation was observed, therefore all deflections measured in this work can be assumed to be purely elastic.

The second in-situ measurement was carried out on the same NW immediately after the manipulation with the AFM tip. Here the electrically induced mechanical resonance of the NW was studied by positioning the edge of a tungsten tip above the free end of the NW at a distance of a few hundred nanometers (z). The tip was mounted on a second nanomanipulator arm. An electric field is applied between the tip and the NW containing both direct and alternating components with tunable frequency. The electrostatic force acting between the tip and the NW (F_{cap}) can be described by considering the capacitance (C) of the whole tip-NW system

$$F_{cap}=\frac{1}{2}\frac{dC}{dz}V^2 \tag{1}$$

where V is the sum of the applied potential and the contact potential between the tip and the NW (V_{CPD})

$$V=(V_{DC}-V_{CPD})+V_{AC}\sin(2\pi\upsilon t) \tag{2}$$

V_{DC} (1.36 V) is the direct part, and V_{AC} (1 V) is the alternating part of the applied electric field having a frequency of ν. If the applied frequency matches the natural resonance frequency of the NW, it leads to mechanical oscillation of the NW. Hence by sweeping the applied frequency the resonance frequency can be determined. We examined the first harmonic oscillation in each case.

3. Results and discussion

The SEM study revealed that the NWs are perpendicularly standing on their substrate (Fig. 2a) and having hexagonal cross sections which are collectively aligned. According to image analysis the average length and diameter are 9.6 ± 3.1 μm and

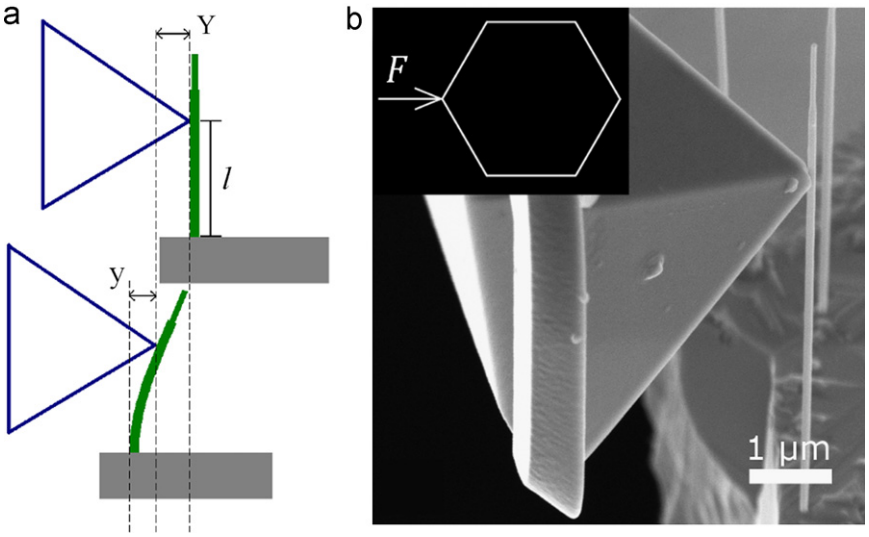

Fig. 1. Schematic of the static bending test on a single InAs nanowire. Snapshots were taken in relaxed and stressed states to determine both cantilever and nanowire deflections (Y and y, respectively) and the vertical position of the applied load (l) (a). The corresponding scanning electron micrograph of the measurement (b). The inset in the latter indicates that the bending load was applied in the $\langle 11–20\rangle$ crystallographic direction.

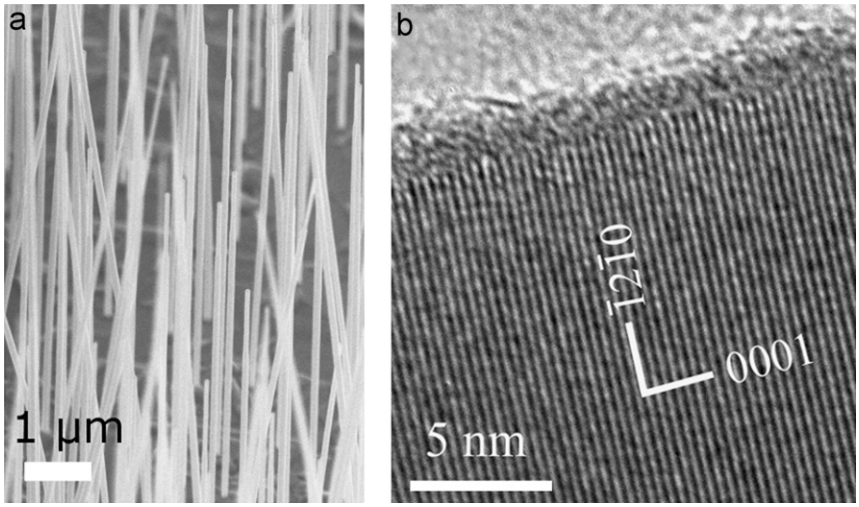

Fig. 2. Electron microscopy images of InAs nanowires grown by molecular beam epitaxy on an InAs(111)B substrate. Tilted view (45°) scanning electron micrograph of vertical InAs nanowire array (a), high resolution TEM image of individual nanowire indicating that the [0001] direction is parallel to the longitudinal axis (b).

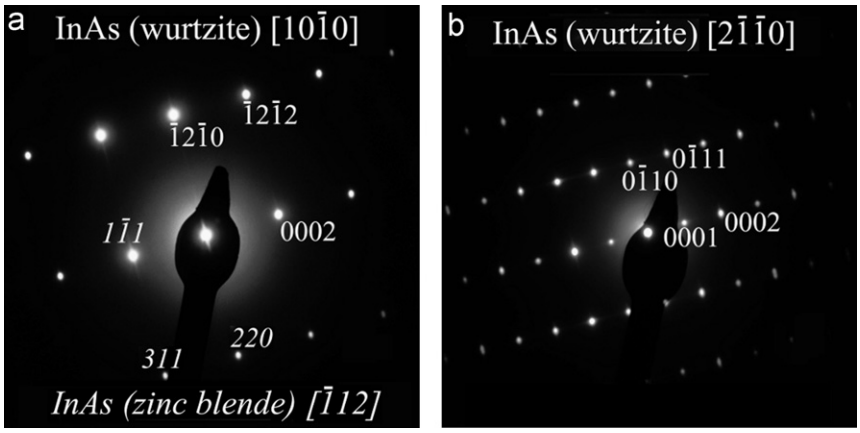

Fig. 3. Selected area electron diffraction patterns revealed during a tilting experiment in the TEM. The SAED in (a) was taken before tilting the NW. It can be indexed by both the cubic and hexagonal structures depicted by italic and normal characters, respectively. The SAED in (b) was taken after tilting the NW by 30° around its longitudinal axis. It can be indexed based exclusively on the hexagonal system. This confirms the hexagonal wurtzite structure of the InAs nanowires and rules out cubic zinc blende stacking.

93 ± 11 nm, respectively. The cross section along the vertical axis is homogeneous except a thinner, but also homogeneous part at the top of the NW, which constitutes around 15% of the whole length. Due to the growth method, a hemispherical gold catalyst particle remained at the free end of the NWs.

The TEM and selected area electron diffraction (SAED) observation revealed that the NWs are wurtzite type single crystals of high quality, where the longitudinal axis is parallel to the [0001] direction. We examined several NWs, and they exhibited wurtzite structure along the whole length with only few planar defects, even at the bottleneck shaped transition between the thinner and thicker parts of the NWs. Figs. 3a and 2b show the SAED pattern and the corresponding high resolution TEM image taken from the middle of the NW. It should be noted that since the SAED patterns at certain orientations can be indexed considering both cubic and hexagonal structures, one could confuse zinc-blende and wurtzite type InAs (both indexing are indicated in Fig. 3a). Therefore, we have paid attention to tilt the NW in the TEM, starting from the $z=[10-10]$ zone axis of hexagonal by 30° around the [0001] direction (this would correspond to tilting from $z=[-112]$ around [111] in the cubic system). The so revealed SAED pattern shown in Fig. 3b can be indexed only on the base of hexagonal structure. That excludes cubic zinc blende and confirms that our InAs NWs are of hexagonal wurtzite type.

We randomly selected five InAs NWs which were standing near the sample edge and they were mechanically tested using both static bending and dynamic excitation methods. In Table 1 the obtained NW and cantilever deflection values (y, Y) and the vertical position of the applied load (l) in the static and the resonance frequencies in the dynamic experiments (ν_{rez}) are listed with the corresponding geometrical parameters.

A typical resonance curve obtained with NW#2 is plotted in Fig. 4a. The amplitude values in the frequency range around the resonance were determined from image snapshots (Fig. 4b and c). The quality factor of the resonance ($Q=\nu_{rez}/\Delta\nu$) is 1260, therefore the system is considerably underdamped.

The bending modulus of the NWs were at first determined from the static mechanical test. The magnitude of the bending load can be calculated by multiplying the AFM cantilever deflection (Y) and its spring constant (k_{SiN}),

$$F = k_{SiN} Y \tag{3}$$

k_{SiN} was determined experimentally using a reference cantilever to avoid the calculations with the geometry and Young's modulus

of silicon nitride, which is spreading in a wide range in the literature. Here the cantilever to be calibrated is used to record a force curve at the very end of the reference beam as well as on a hard surface. The slope of the contact portion of the two force curves (i.e. the deflection sensitivity) can be used to calculate the spring constant [16]

$$k_{SiN} = k_{ref}\left(\frac{S_{ref}}{S_{hard}} - 1\right) \tag{4}$$

where k_{ref} is the spring constant of the reference cantilever, S_{ref} and S_{hard} are the deflection sensitivities measured on the reference cantilever and on a hard surface, respectively. We obtained a spring constant of 2.34×10^{-2} N/m. Since the bending load was applied below the thinner top part of the NW in the case of all five NWs (Fig. 1a), we calculated the BM by solving the static Euler–Bernoulli equation for a uniform cross section

$$E_{BM} = \frac{Fl^3}{3yI} \tag{5}$$

where l is the vertical position of the applied load and I is the second moment of inertia. I can be calculated by assuming a hexagonal cross section

$$I = \frac{5\sqrt{3}a^4}{16} \tag{6}$$

where a is the edge of the hexagon. The obtained bending moduli range from 32 to 67 GPa, as shown in Fig. 5 (blue circles). The error bars are estimated according to Gauss's error propagation law assuming that the uncertainty of the quantities equals twice the pixel size of the corresponding SEM image. The mean BM, i.e. Young's modulus in the [0001] direction is 43.5 ± 14 GPa, where $\pm$ indicates the standard deviation of the measurements.

The BM of each NW was also determined from the resonance frequencies. Contrary to the bending experiment, here the mechanical model with uniform cross section is not adequate, and the upper thinner part has to be also taken into account. Thus the finite element method (FEM, Comsol Multiphysics) was used where the NWs were modeled by considering their real geometry according to SEM analysis, i.e. the thicker part at the bottom, the thinner part at the top (Table 1) and the gold catalyst particle at the very end of the NWs. The bottom of the NWs was anchored in the model. The optimal mesh density is determined by gradually increasing the mesh density starting with a coarse mesh. We continued refining the mesh as long as any increasing in the mesh density had an impact on the final results. We applied a mass density of 5480 kg/m^3 calculated using the lattice parameters of wurtzite InAs (a=4.327 Å and c/a=1.639) [17]. The BM was determined by solving an inverse problem, i.e. the resonance values were calculated by sweeping the young's modulus in the model until a good agreement is reached with the experimental value.

The obtained bending moduli for the resonance experiments agree well with the values obtained in bending experiment (Fig. 5) except for NW#4, where the BM from the resonance excitation technique considerably is out of the error range of the corresponding static BM.

Table 1
Geometrical parameters of the examined InAs nanowires: length of the bottom part (L_1), length of the top part (L_2), diameter of the bottom part (D_1) and diameter of the top part (D_2). Vertical position of the applied load (l), nanowire deflections (y), the corresponding cantilever deflections (Y), and the resonance frequencies provided by the resonance excitation technique (ν_{rez}). Note that the nanowires are built up from a thicker lower and a thinner upper segment. The measured diameter corresponds to the double of the edge of the hexagonal cross section.

NW #	L_1 (μm)	L_2 (μm)	D_1 (nm)	D_2 (nm)	l (μm)	y (nm)	Y (nm)	ν_{rez} (kHz)
#1	7.37	1.20	103	68	4.50	343	71	522.3
#2	7.06	1.01	98	66	4.70	691	85	567.1
#3	6.34	1.12	93	68	5.58	588	40	559.0
#4	6.91	1.04	93	68	5.61	726	89	542.1
#5	4.53	1.16	102	73	3.43	561	285	1138.7

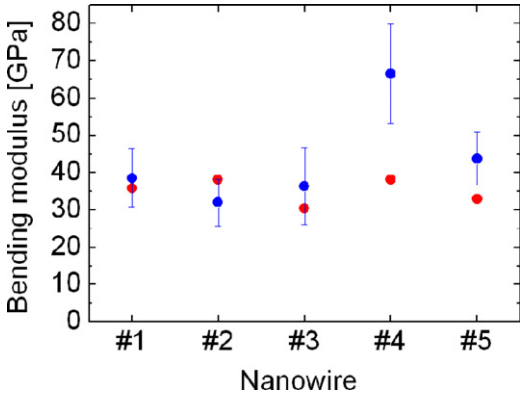

Fig. 5. (Color online) Bending modulus values of InAs nanowires provided by the in-situ bending experiment (blue circles with error bar) and the finite element method (red circles) considering the experimentally obtained resonance frequencies from the resonance excitation method.

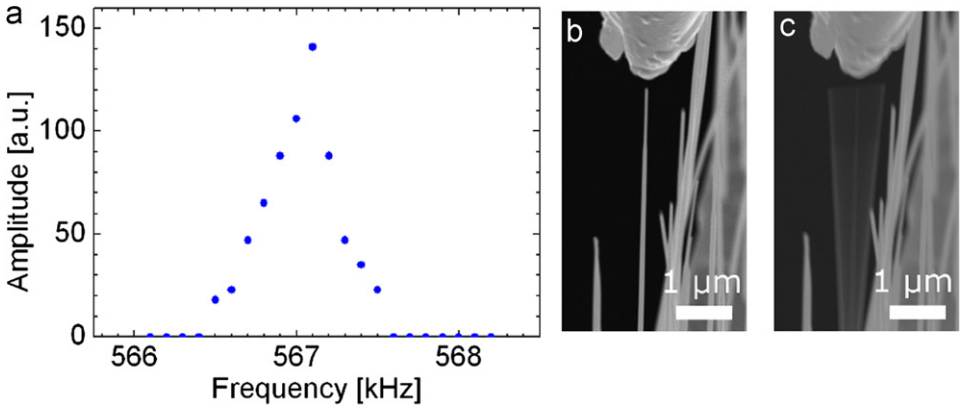

Fig. 4. Resonance excitation of nanowire #2 using alternating electric field. (a) Amplitude resonance measured on the SEM snapshots taken around the natural resonance (567.1 kHz) and the two typical SEM images recorded (b) far from the natural resonance frequency of the nanowire and (c) at the resonance frequency. Note that the quality factor is considerably high (1260).

However, the degree of this discrepancy is far below the deviation of Young's modulus values of other wurtzite, e.g. ZnO NWs reported in the literature [7]. This indicates that the resonance technique confirms the results of the static bending test. Therefore both the bending technique and Young's modulus of 43.5 GPa of wurtzite InAs NWs is validated. This value is significantly lower than Young's modulus of zinc-blende bulk InAs in the [111] direction ($E_{111}=97$ GPa). Since wurtzite InAs does not exist in bulk form, there are no experimental data for Young's modulus on this. Only theoretical calculations exist, and they predict no difference in Young's modulus for wurtzite and zinc-blende crystals [18].

Part of the deviation from the bulk value of zinc blende Young's modulus might be explained by softening at the surfaces [19]. Also the high quality wurtzite NWs may be the reason for the decreased bending modulus. Both of these issues are also addressed and in agreement with data presented by Lexholm et al. [12]. Park et al. has summarized mechanical properties for different types of nanowires and concludes that there are a huge gap between theoretical and experimental values of Young's modulus [20].

Besides, it is also seen from the resonance in Fig. 4a that the high quality wurzite NWs are suitable for ultra sensitive mass measurement by attaching a small particle to the free end of the NW and measuring the frequency shift. The calculated sensitivity of the vibrating cantilever balance at the first harmonic mode can be estimated by the following equation [3]:

$$\Delta M_p \approx \frac{6}{\beta_1^4 Q} M_0 \tag{7}$$

where $\beta_1=1.875$ is the constant for the first harmonic vibration and M_0 is the mass of the NW. For NW#2 with $M_0=1.24$ pg, the lowest estimated mass which can be measured is 0.477 fg.

Although as it turned out the two in situ methods lead to the very similar result both of them have advantages and disadvantages. While with the resonant excitation only high aspect ratio NWs can be characterized the static bending technique can be applied even for low aspect ratio (<20) and rigid NWs and nanorods. Furthermore the latter method does not depend on the electrical properties of the NWs to be measured. Moreover, with the bending technique it is also possible to investigate the change of the Young modulus along the axis of the NW by taking a series of bending experiments at different vertical load positions. On the other hand for homogenous, high aspect ratio NWs the resonant method can be easier since it is no need to carefully calibrate and prepare the probe. Moreover, the resonance excitation technique can provide the quality factor of the oscillating NW system.

4. Summary

In conclusion, we have presented a general combined method for measuring the bending modulus of individual cantilevered nanostructures applying two nanomanipulator arms in the SEM. One is responsible for a static bending test, and the other one is used to electrically excite mechanical oscillations. The dynamic experiment validates the result of the static bending test. Up to our knowledge this is the first time, that the two techniques are applied on the same individual nanostructures to cross-confirm the results. Moreover, the mechanical properties of wurtzite InAs NWs have been characterized by this method. Young's modulus in the [0001] direction was measured to be 43.5 GPa, which is significantly lower, than that of cubic bulk InAs in the [111] direction. The high resonance quality factor (1260) of the wurtzite InAs NWs makes the material a promising candidate for sub-femtogram mass detectors.

Acknowledgments

This work was supported by the Hungarian Fundamental Research Found (OTKA) under contracts PD77578 and K76287, by the EU FP7 project SE2ND, by the János Bólyai Research Scholarship of the Hungarian Academy of Sciences as well as by the National Development Agency grant TÁMOP-4.2.2/B-10/1-2010-0025. Nanowire synthesis was supported by UNIK Synthetic Biology and the CLIPS project of the Danish Strategic Research Council. We acknowledge the valuable discussions with O. Geszti, and G. Radnóczi. We are grateful to L. Illés for SEM experiments and to P. Krogstrup and C.B. Sørensen for assistance on MBE growth.

References

[1] Y. Huang, X. Bai, Y. Zhang, J. Phys.: Condens. Matter 18 (2006) L179.
[2] Y. Huang, Y. Zhang, X. Wang, X. Bai, Y. Gu, X. Yan, Q. Liao, J. Qi, J. Liu, Cryst. Growth Des. 9 (2009) 1640.
[3] A.V. Desai, M.A. Haque, Sens. Actuators A-Phys. 134 (2007) 169.
[4] R. Agrawal, B. Peng, E.E. Gdoutos, H.D. Espinosa, Nano Lett. 8 (2008) 3668.
[5] B. Wen, J.E. Sader, J.J. Boland, Phys. Rev. Lett. 101 (2008) 175502.
[6] S. Hoffmann, F. Östlund, J. Michler, H.J. Fan, M. Zacharias, S.H. Christiansen, C. Ballif, Nanotechnology 18 (2007) 205503.
[7] M.P. Manoharan, A.V. Desai, G. Neely, M.A. Haque, J. Nanomater. 2008 (2008) 849745.
[8] M.-R. He, Y. Shi, W. Zhou, J.W. Chen, Y.J. Yan, J. Zhu, Appl. Phys. Lett. 95 (2009) 091912.
[9] P. Poncharal, Z.L. Wang, D. Ugarte, W.A. de Heer, Science 283 (1999) 1513.
[10] A.G. Milnes, A.Y. Polyakov, Mater. Sci. Eng. B 18 (1993) 237.
[11] S.O. Mariager, D. Khakhulin, H.T. Lemke, K.S. Kjær, L. Guerin, L. Nuccio, C.B. Sørensen, M.M. Nielsen, R. Feidenhans'l, Nano Lett. 10 (2010) 2461.
[12] M. Lexholm, I. Karlsson, F. Boxberg, D. Hessman, Appl. Phys. Lett. 95 (2009) 113103.
[13] M. Koguchi, H. Kakibayashi, M. Yazawa, K. Hiruma, T. Katsuyama, Jpn. J. Appl. Phys. 31 (1992) 2061.
[14] P. Caroff, K.A. Dick, J. Johansson, M.E. Messing, K. Deppert, L. Samuelson, Nat. Nanotechnol. 4 (2009) 50.
[15] H. Shtrikman, R. Popovitz-Biro, A. Kretinin, L. Houben, M. Heiblum, M. Bukała, M. Galicka, R. Buczko, P. Kacman, Nano Lett. 9 (2009) 1506.
[16] 〈http:/nanoscaleworld.bruker-axs.com/nanoscaleworld〉.
[17] H. Shu, X. Chen, H. Zhao, X. Zhou, W. Lu, J. Phys. Chem. C 114 (2010) 17514.
[18] R.M. Martin, Phys. Rev. B 6 (1972) 4546.
[19] L.G. Zhou, H. Huang, Appl. Phys. Lett. 84 (2004) 1940.
[20] H.S. Park, W. Cai, H.D. Espinosa, H. Huang, MRS Bull. 34 (2009) 178.